이학석사 학위논문

A Feasibility Study of Cell Membrane Engineering for PSMA-Targeted Cell Therapy and Trafficking

PSMA 표적 세포치료 및 세포추적을 위한

세포막공학 연구

2023 년 **2** 월

서울대학교 융합과학기술대학원

응용바이오공학과

김 혜 원

A Feasibility Study of Cell Membrane Engineering for PSMA-Targeted Cell Therapy and Trafficking

지도교수 김 상 은

이 논문을 이학석사 학위논문으로 제출함

2023 년 **2** 월

서울대학교 융합과학기술대학원

응용바이오공학과

김 혜 원

김 혜 원의 이학석사 학위논문을 인준함

2023년 **2**월

위 원 장 이 원 우 (인)

부 위 원 장 김 상 은 (인)

위 원 박 현 수 (인)

Abstract

A Feasibility Study of Cell Membrane Engineering for PSMA-Targeted Cell Therapy and Trafficking

Hye Won Kim
Department of Applied Bioengineering
Graduate School of Convergence Science and Technology
Seoul National University

Cell therapy is based on cells such as stem cells and immune cells. In particular, immunomodulatory cell therapy treats diseases by activating the immune response using immune cells such as dendritic cells, natural killer cells, and T-cells. Among them, a concept of introducing a gene expressing a chimeric antigen receptor into T cells (CAR-T) has been developed recently for cancer treatment and is expected to be approved internationally. However, these CAR-T-based therapies have some limitations due to side effects of on-target/off-tumor effects when adequate targeting is not achieved. To overcome the limitations and side effects of these targeting capabilities, efforts are being made to develop bispecific CAR-T cells or to improve the performance and efficacy of CARs.

Metabolic glycoengineering is a technology that can introduce receptors that can be chemically labeled on the cell surface using artificial sugar and glycoprotein

synthesis. Reactive azide groups can be formed on the cell surface for chemical labeling using a substrate such as N-azidoacetyl-mannosamine ($Ac_4ManNAz$). After that, it can easily and quickly combine various structures that be conjugated by bioorthogonal chemical reactions *in vitro* or *in vivo*.

This study aimed to increase the targeting ability against PSMA in cell therapy using metabolic glycoengineering and "click reaction" and visualize cell trafficking using PET imaging.

THP-1 cells were incubated with $Ac_4ManNAz$ at various concentrations (0, 5, 10, 20, 50, and 100 μM) for 24 h to incorporate reactive functional groups on the cell surface. Metabolically glycoengineered cells were stained by DBCO-bearing fluorophore (ADIBO-Cy5.5) for 1 h at different concentrations (0, 5, 10, 20, 50, and 100 μM) and analyzed by confocal fluorescence microscopy and flow cytometric assay. For PSMA ligand attachment to THP-1 cells, $Ac_4ManNAz$ treated THP-1 cells were incubated with DBCO-PSMA ligand (ADIBO-GUL) at a final concentration of 100 μM for 1 h. To evaluate the effect on cell recognition, PSMA ligand-armed THP-1 cells (as effectors) were co-cultured with PSMA-positive, 22RV1 cells or PSMA-negative, PC3 cells (as target cells) at a 3:1 effector-to-target cell (E/T) ratio. The interaction between THP-1 and target cells was monitored by confocal fluorescence microscopy. THP-1 cells were used without a PSMA targeting motif as a negative control. $[^{89}Zr]Zr(oxinate)_4$ was prepared from its oxalate form by using an anion exchange "sep-pak" cartridge. $LogD_{7.4}$ assay was performed to confirm the lipophilicity of the synthesized $[^{89}Zr]Zr(oxinate)_4$. For preparing the radiolabeled THP-1, the cells were treated at the activity level of ~740 kBq of $[^{89}Zr]Zr(oxinate)_4/5\times10^6$ cells. Radiolabeled cells were analyzed for determination of cell-associated radioactivity by gamma

counting and cell viability was measured up to 7 day by MTS assay. PSMA targeting ligand armed THP-1 cells radiolabeled with [^{89}Zr]Zr(oxinate)$_4$ was injected into normal mice through the tail vein. PET images were obtained at 2 hours, 1, 4, and 6 days after injection.

In the cytotoxicity assay, THP-1 cells did not present cytotoxicity even when the Ac$_4$ManNAz or ADIBO-Cy5.5 treated concentration was 100 μM. In confocal imaging and flow cytometric assay, ADIBO-Cy5.5 efficiently labeled THP-1 cells in a dose-dependent manner, and the dose of 100 μM was the optimum concentration for the following experiments. Intercellular gluing was not observed in PSMA negative PC3 cells. 22RV1 cells did not show cell-to-cell gluing with non-armed THP-1 cells. However, the clusters of PSMA ligand-armed THP-1 cells and 22RV1 were identified, indicating cell-cell recognition over the cell surface between two types of cells. LogD$_{7.4}$ of [^{89}Zr]Zr(oxinate)$_4$ was determined as 1.47 ± 0.02. Cell radiolabeling efficiency was 54.5 ± 17.8%. THP-1 labeled with 0.09 ± 0.03 Bq/cell showed no significant cytotoxicity compared to unlabeled THP-1 up to 7 days. Injected THP-1 cells accumulated in the lung and gradually moved to other organs, such as the liver and spleen, over time.

Ac$_4$ManNAz treated cells were prepared efficiently and labeled with ADIBO-GUL for preparing the PSMA-targeted cells. [^{89}Zr]Zr(oxinate)$_4$ can be used to label cells without toxicity. The study results suggest that PSMA-ligand armed cell therapy could improve cell targeting efficacy and be monitored by PET imaging.

Keyword: Cell therapy, PSMA, Metabolic glycoengineering, Click chemistry, Cell trafficking, PET

Student Number: 2019-27624

Table of Contents

Figure legends

Figure 1.1 Schematic illustration of cell labeling via metabolic glycoengineering. Ac_4ManNAz is taken up by cells and incorporated into membrane proteins, resulting in the metabolic labeling of membrane proteins with azide.

Figure 1.2 Schematic illustration of the generated azide groups after Ac_4ManNAz treatment and bioorthogonal copper-free click chemistry for cell labeling.

Figure 1.3 Schematic representation of the $[^{89}Zr]Zr(oxinate)_4$ synthesis.

Figure 1.4 Schematic illustration of developing various Lys-urea-Glu scaffold-based radiolabeled PSMA targeting inhibitors.

Figure 2.1 *In vitro* cytotoxicity of THP-1 cells at various concentrations of Ac_4ManNAz.

Figure 2.2 *In vitro* cytotoxicity of THP-1 cells at various concentrations of DBCO-Cy5.5.

Figure 2.3 Differences in the efficiency of bioorthogonal labeling according to the DBCO-Cy5.5 treatment concentration. (A) Confocal microscopy analysis of Ac_4ManNAz treated THP-1 cells after DBCO-Cy5.5 conjugation at various concentrations. The merged image showed Cy5.5(red) localized on the cellular membrane. (B) Flow cytometric assay of Ac_4ManNAz treated THP-1 cells after DBCO-Cy5.5 conjugation at various concentrations. Fluorescence intensity increased in a dose-dependent manner of DBCO-Cy5.5.

Figure 2.4 Cell-to-cell gluing test. Target cells(PC3 and 22RV1 cells) were stained with Far-Red dye(red), and effector cells(THP-1 cells) were stained CFSE(green), respectively.

Figure 2.5 Cytotoxicity of radiolabeled cells at different radioactivity conditions. Radiolabeling under low activity conditions significantly increased cell viability until day 3, after that, showed no difference from the negative control. However, under high activity conditions, it was determined that cell viability was slightly increased on day 1 and then decreased rapidly by cytotoxicity.

Figure 2.6 Representative small animal PET/CT images at 2, 24, 96, and 144 h after injection of radiolabeled armed THP-1 cells in normal mice.

Table legends

Table 1. Initial cell number of radiolabeled THP-1 for daily cytotoxicity assay.

Chapter 1. Introduction

1.1. Cell therapy

Cell therapy is rapidly evolving as cell-based therapy, including stem cells and immune cells. In particular, immunomodulatory cell therapy involves treating diseases by activating the immune response using immune cells such as dendritic cells, natural killer cells, and T-cells. Among them, a concept of introducing a gene expressing a chimeric antigen receptor into T cells (CAR-T) has been developed recently for cancer treatment. Various therapies based on CAR-T are undergoing clinical trials, and some are now licensed for clinical use [1-3]. However, these CAR-T-based therapies have limitations due to side effects of on-target/off-tumor effects when adequate targeting is not achieved [4,5]. To overcome the limitations and side effects of these targeting capabilities, efforts are being made to develop bispecific CAR-T cells or to improve the performance and efficacy of CARs [6-9].

1.2. Bioorthogonal engineering

Metabolic glycoengineering is a technology that can introduce receptors chemically on the cell surface using artificial sugar and glycoprotein synthesis. N-azidoacetyl-mannosamine ($Ac_4ManNAz$) is widely used for engineering the living cell surface. Azide groups can be expressed on the cell membrane for chemical labeling using a substrate such as $Ac_4ManNAz$. $Ac_4ManNAz$ is metabolized into N-azidoacetyl neuraminic acid. Then, it is incorporated into glycans, such that azide groups are expressed in the glycans on the surface of living cells (**Figure 1.1**). As such, metabolic glycoengineering provides binding sites for nanoparticles by creating bioorthogonal chemical receptors on the cell membrane.

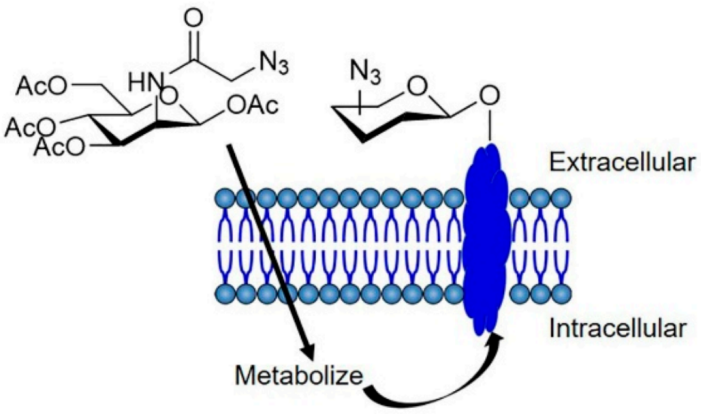

Figure 1.1 Schematic illustration of cell labeling via metabolic glycoengineering. Ac_4ManNAz is taken up by cells and incorporated into membrane proteins, resulting in the metabolic labeling of membrane proteins with azide (reproduced from Nishikawa, M. et al. [10]).

A new strategy for cell trafficking using bioorthogonal copper-free click chemistry has attracted considerable attention for its high specificity and low rate of adverse effects in the cells. Indeed, after azide is expressed on the surface of living cells, tumor-targeting motifs can easily and quickly conjugate to the cell surface using bioorthogonal "click" chemistry in vitro or in vivo (**Figure 1.2**) [11].

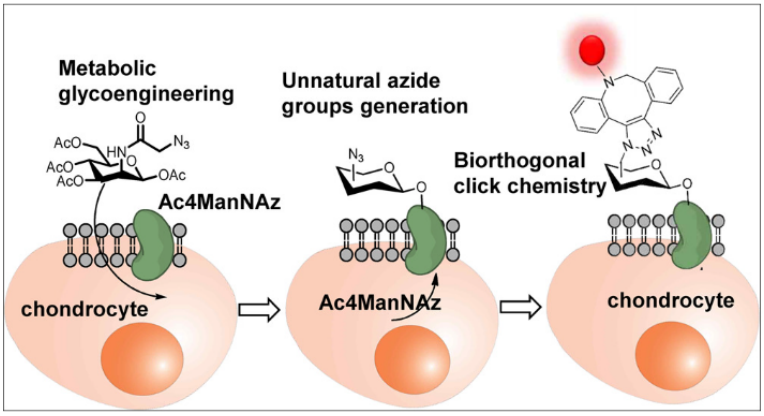

Figure 1.2 Schematic illustration of the generated azide groups after Ac_4ManNAz treatment and bioorthogonal copper-free click chemistry for cell labeling (reproduced from Kwangmeyung, K. et al. [12]).

1.3. Cell trafficking by PET

Non-invasive imaging is ideal for the whole-body quantification and longitudinal monitoring of cellular and molecular processes. Positron emission tomography (PET), a non-invasive imaging tool, can be applied to understand the spatio-temporal dynamics of the trafficking of administered therapeutic cells. PET offers very high sensitivity for monitoring cell trafficking. Only a trace amount of the radiopharmaceutical in the order of picomolar concentrations is needed for detection, pharmacokinetic modeling, and determining the biodistribution of the administered cells [13, 14].

Successful cell trafficking methods for routine clinical applications require tracers with a long half-life, reliable labeling ability, and cellular retention. However, ^{18}F used in [^{18}F]FDG, a radiopharmaceutical currently actively used clinically, is unsuitable for continuous tracking of administered cells due to its short physical half-life (110 minutes). On the other hand, ^{89}Zr can be used to acquire PET images and has a relatively long physical half-life of 78.4 hours, making it suitable for continuous cell tracking [15, 16]. ^{89}Zr has emerged as a promising PET radioisotope for direct cell labeling and has been widely used for antibody-based immuno-PET imaging over the last decade [17]. ^{89}Zr can be used for the synthesis of the neutral and lipophilic complex [^{89}Zr]Zr(oxinate)$_4$ with four oxine (8-hydroxyquinoline) ligands bound to ^{89}Zr that enter cells through passive mechanisms (**Figure 1.3**).

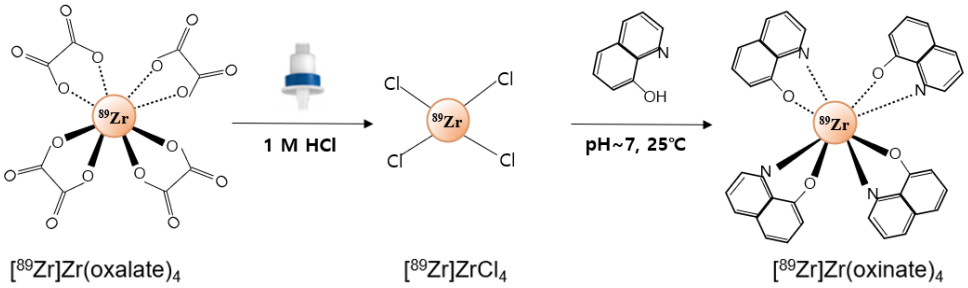

Figure 1.3 Schematic representation of the [^{89}Zr]Zr(oxinate)$_4$ synthesis.

1.4. Prostate-specific membrane antigen(PSMA)

Prostate-specific membrane antigen (PSMA) is a human protein, and its regular tissue expression is restricted to a few organs [18]. However, its expression is further increased, especially in prostate cancer, attracting attention as a specific target molecule for diagnosing and treating prostate cancer [19-21]. Various small-molecular compound-based PSMA inhibitors have been developed and studied as agents for targeting PSMA for imaging and diagnostic therapy. Among these radiopharmaceuticals, [^{68}Ga]Ga-PSMA-11 and [^{18}F]F-DCFPyl have been approved by the US Food and Drug Administration for diagnosis and are used clinically [20].

Among various small molecule PSMA inhibitors, a urea-based ligand is the most widely used structure, which is stable and has a high affinity for PSMA [22]. Most small molecule PSMA inhibitors for diagnosis and treatment have a PSMA-targeting peptide, glutamine-urea-lysine (GUL), a chelator capable of binding a metallic radioisotope, and a spacer. As a PSMA targeting pharmacophore, GUL can bind to various ligands, radioisotopes, or cytotoxic anticancer drugs through modification (**Figure 1.4**) [23, 24].

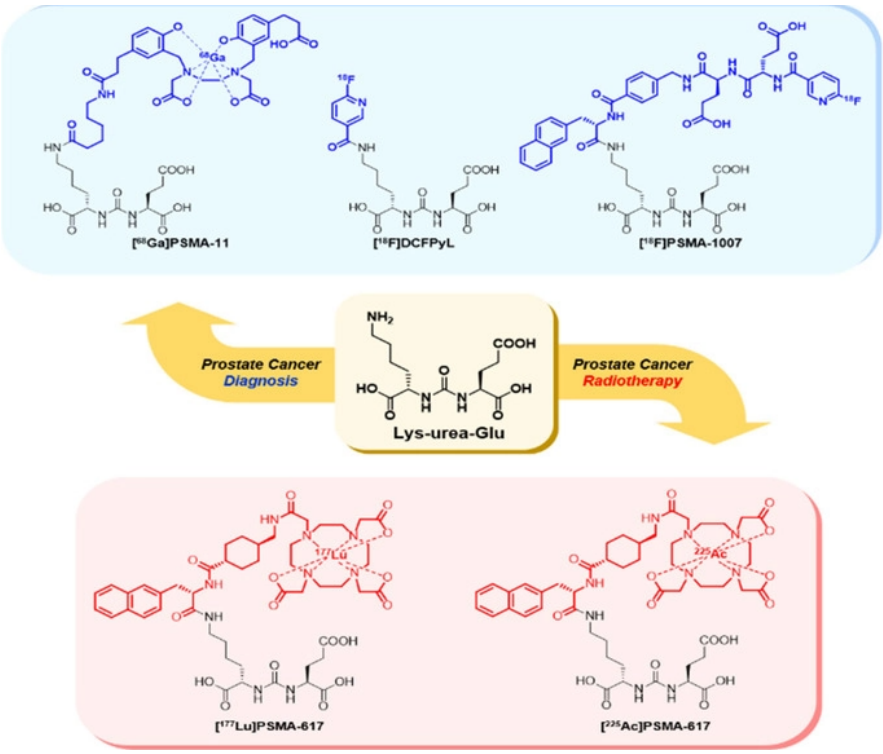

Figure 1.4 Schematic illustration of developing various Lys-urea-Glu scaffold-based radiolabeled PSMA targeting inhibitors (reporduced from Kwon et al. [24]).

1.5. Research objectives

In this study, THP-1 cells were modified to enhance the targeting ability for PSMA-positive tumor cells using metabolic glycoengineering and bioorthogonal "click" chemistry. In addition, THP-1 cells were radiolabeled with $[^{89}Zr]Zr(oxinate)_4$ for PET imaging that could track their migration in vivo.

Chapter 2. A feasibility study of cell membrane engineering for PSMA-targeted cell therapy and trafficking

2.1. Background

Cell therapy is based on cells such as stem cells or immune cells. In particular, immunomodulatory cell therapy treats diseases by activating the immune response using immune cells such as dendritic cells, natural killer cells, and T-cells. CAR-T, a novel immunomodulatory cell therapy involving the introduction of genes expressing chimeric antigen receptors (CARs) into T cells, has recently been actively researched clinically and is expected to be approved internationally. However, these CAR-T-based therapies also have limitations due to side effects of on-target/off-tumor effects when sufficient targeting is not achieved. To overcome the limitations and side effects of these targeting capabilities, efforts are being made to develop bispecific CAR-T cells or to improve the performance and efficacy of CARs.

Cell-cell interactions between immune cells and tumor cells are essential to overcome the problems of CAR-T-based immune cell therapy. More effective anticancer treatment can be expected if the binding between these two types of cells is enhanced. In particular, binding between ligands and receptors on the cell surface plays an important role [25]. For example, CD20, CD22, HER2, etc., used for CAR-T, are employed for targeting tumor cells [26, 27]. Recently, a method of controlling glycostructure expression on the cell surface using metabolic glycoengineering and binding structures such as artificial target ligands using bioorthogonal “click” chemistry has been proposed [28, 29].

Metabolic glycoengineering is a technology that can introduce receptors chemically on the cell surface using artificial sugar and glycoprotein synthesis. A reactive azide group can be expressed on the cell membrane for chemical labeling using a substrate such as N-azidoacetyl-mannosamine ($Ac_4ManNAz$). After that, it can easily and quickly combine with various structures that can be conjugated through bioorthogonal chemical reactions *in vitro* or *in vivo*.

2.2. Experimental

2.2.1. Materials

$Ac_4ManNAz$, carboxyfluorescein succinimidyl ester (CFSE), Far-red solution, 4′,6-diamidino-2-phenylindole (DAPI) were purchased from Thermo Fisher Scientific (MA, USA). ADIBO-Cy5.5 was purchased from FutureChem (South Korea). The MTS/PMS solution for the cytotoxicity test was purchased from Promega(MS, USA). RPMI-1640 cell culture medium was purchased from Welgene (South Korea). PBS, 8-hydroxyquinoline (8-HQ), 2-mercaptoethanol, and fetal bovine serum (FBS) were purchased from Sigma-Aldrich (MA, USA). Dulbecco's Phosphate Buffered Saline (DPBS), trypsin, and antibiotic-antimycotic were purchased from Gibco (MO, USA). THP-1 cell, a monocyte isolated from peripheral blood from an acute monocytic leukemia patient, was purchased from Korean Cell Line Bank (KCLB, South Korea). 22RV1 and PC3 cells, human prostate carcinoma epithelial cell lines, were purchased from the American Type Culture Collection (ATCC).

2.2.2. Cell culture

THP-1 cells were cultured in RPMI-1640 cell culture medium, supplemented with 10% FBS, 1% antibiotic-antimycotic, and 0.05 mM of 2-mercaptoethanol. THP-1 cells were maintained in suspension in a standard CO_2 incubator (5% CO_2,

37°C). 22RV1 and PC3 cells were cultured in RPMI-1640 medium, supplemented with 10% FBS and 1% antibiotic-antimycotic. 22RV1 and PC3 cells were maintained in suspension in a CO_2 incubator.

2.2.3. *In vitro* cytotoxicity assay

Cytotoxicity was evaluated using the MTS assay after treatment with $Ac_4ManNAz$ or DBCO-Cy5.5, respectively. To determine the optimal concentration of $Ac_4ManNAz$ for THP-1 cells, THP-1 cells were seeded onto 96-well plates (1.0×10^5 cells/100 μl/well, $n = 5$) and incubated with various concentrations (0, 5, 10, 20, 50, or 100 μM) of $Ac_4ManNAz$ for 24 h. After incubation, the medium was discarded, and the cells were washed twice with DPBS. MTS solution (20 μl/100 μl of cell culture media) was added to each well. After a 2 h incubation, the absorbance of each well was measured at 490 nm and a reference wavelength of 700 nm using a microplate reader (SpectraMax Plus 384, Molecular Devices Corp., SJ, USA).

To assess the cell viability, THP-1 cells were treated with DBCO-Cy5.5 (0, 5, 10, 20, 50, or 100 μM for 1 h). After incubation, the medium was discarded, and the cells were washed twice with DPBS. MTS solution (20 μl/100 μl of cell culture media) was added to the DBCO-Cy5.5-treated THP-1 cells and incubated for 2 h. The absorbance of DBCO-Cy5.5-treated THP-1 cells was measured at 490 nm, with a reference wavelength of 700 nm. The cell viability was calculated according to *Eq*. 1:

$$Cell\ viability\ (\%) = \frac{OD_{Treatment}}{OD_{Contorl}} \times 100\% \cdots\cdots Eq.1$$

where $OD_{Treated}$ and $OD_{Control}$ refer to the optical density of each treated condition and 0 μM treated of $Ac_4ManNAz$ or DBCO-Cy5.5.

2.2.4. *In vitro* azide generation and bioorthogonal labeling of THP-1 cells

In vitro, cell-surface azide expression and bioorthogonal labeling strategy were used to increase the tumor-targeting ability of THP-1 cells. Confocal fluorescence microscopy and flow cytometric assay were conducted to monitor azide generation and bioorthogonal labeling. THP-1 cells (1.0×10^6 cells/1.2 ml) were incubated with a final concentration of 100 μM of Ac_4ManNAz for 24 h in a 24-well plate. Then, THP-1 cells were transferred to a FACS tube and centrifuged at 130×g for 5 min, at 37°C, and the cell pellets were washed twice with DPBS. The azide-expressing THP-1 cells were treated with various concentrations (0, 5, 10, 20, 50, or 100 μM) of ADIBO-Cy5.5 for 1 h, at 37°C in a CO_2 incubator. Cy5.5 treated THP-1 cells were washed twice with DPBS, and the cell pellets were resuspended in DPBS, including 1% bovine serum albumin for flow cytometric assay. Flow cytometry was performed at Ex: 633 nm/ Em: 667 nm. Furthermore, Cy5.5 treated THP-1 cells were treated with DAPI for 10 minutes and then fixed in a 4% paraformaldehyde solution for 30 minutes. DAPI-stained Cy5.5-THP-1 cells were examined using confocal fluorescence microscopy (LSM 800, Zeiss, Germany).

2.2.5. Cell-to-cell gluing test

The azide-expressing THP-1 cells that had undergone bioorthogonal labeling with ADIBO-GUL were named "armed" THP-1 cells. The GUL (glycine-urea-lysine) motif on the cell surface increases the targeting ability for PSMA. THP-1 cells were treated with 100 μM of Ac_4ManNAz for 24 hours to enable azide-group expression on the cell surface. Next, the azide-expressing THP-1 cells were centrifuged at 130×g for 5 min, and the cell pellets were washed twice with DPBS. To conjugate the azide-expressing THP-1 cells with the PSMA targeting motif, they were treated with 100 μM of ADIBO-GUL for 1 hour. Non-armed THP-1 cells

were only treated with $Ac_4ManNAz$ as a negative control. Armed and non-armed THP-1 cells were monitored using a cell-to-cell gluing test after CFSE staining. Armed and non-armed THP-1 cells (1.5×10^6 cells) were stained with 1.1 μM of CFSE for 20 min at 37°C. Both CFSE-stained armed and non-armed THP-1 cells were washed twice with DPBS.

22RV1 (PSMA positive) and PC3 (PSMA negative) cells were used to determine cell-to-cell gluing by the GUL motif for PSMA-targeted binding. To evaluate the effect on cell recognition, PSMA ligand conjugated THP-1 cells (as effectors) were co-cultured with PSMA positive 22RV1 cells (as target cells) at a 3:1 effector-to-target cell (E/T) ratio. The interaction between THP-1 and 22RV1 was monitored using confocal fluorescence microscopy. The target cells were planted into 6-well plates (5.0×10^5 cells/well, $n = 3$) and incubated for adhesion to the bottom of the plate for 24 h at 37°C in a CO_2 incubator. After incubation, the target cells were treated with 1 mL/well of Far-red solution (0.167 μM) for 20 minutes in a dark place. After incubation, the far-red solution was discarded, and the target cells were washed twice using complete growth media. Finally, the growth medium was replaced with 1 ml of fresh growth medium.

For the cell-to-cell gluing test, the target cells' culture media was removed. Each well was treated with 1.5×10^6 cells/1 ml of armed or non-armed THP-1 cells. After a 4 h co-culture incubation, the supernatant was discarded to remove non-adherent THP-1 cells and washed twice with 3 ml of DPBS. Each well was fixed in 4% paraformaldehyde solution for 30 min at room temperature. Afterward, the 4% paraformaldehyde was removed, and confocal fluorescence microscopy was used to identify whether the effector cells and target cells coexisted through cell-to-cell adhesion.

2.2.6. $[^{89}Zr]Zr(oxinate)_4$ synthesis and radio-TLC

[^{89}Zr]Zr(oxinate)$_4$ complex was synthesized from [^{89}Zr]Zr(oxalate)$_4$ using ion exchange chromatography. Sep-Pak Light Accell plus QMA strong anion exchange cartridge (Waters, MA, USA) was activated with 6 ml of acetonitrile, 10 ml of saline, and 10 ml of distilled water (DDW). A water-diluted [^{89}Zr]Zr(oxalate)$_4$ solution (~ 18.5 MBq/10 mL) was passed through the activated anion exchange cartridge. [^{89}Zr]Zr(oxalate)$_4$ loaded cartridge was washed using more than 100 ml of DDW to remove residual oxalic acid. [^{89}Zr]$ZrCl_4$ was recovered by passing through 300 μL of 1.0 M HCl into the washed cartridge. [^{89}Zr]$ZrCl_4$ was adjusted to a pH of 7.0–8.0 using 1.0 M HEPES buffer, and the pH was confirmed with a pH test paper (Doo-San Scientific, South Korea).

An 8-Hydroxyquinoline (8-HQ) solution was prepared by combining 460 μg of 8-HQ with 1 ml of 10 mM HEPES buffer. 100 μl of the freshly prepared 8-HQ solution was added to [^{89}Zr]$ZrCl_4$ (5 MBq) and incubated at room temperature for 30 min. Radio-TLC (50 mM DTPA, pH 7.0) was conducted to validate the quality of [^{89}Zr]Zr(oxinate)$_4$ complex.

2.2.7. Cell radiolabeling and cytotoxicity

The THP-1 cells (5.0×10^6 cells) were radiolabeled using 0.74 MBq (low activity) or 7.4 MBq (high activity) [^{89}Zr]Zr(oxinate)$_4$ treatment for 30 min (at room temperature, 650 rpm using Thermomixer). The radiolabeled THP-1 cells were washed with 3 ml of complete growth medium twice and PBS once. The radiolabeling efficiency was calculated according to *Eq*. 2:

$$Radiolabeling\ efficiency\ (\%) = \frac{Cell\ pellet\ activity}{Initial\ dose} \times 100\ \% \cdots\cdots Eq.2$$

where cell pellet activity refers to the measured radioactivity using a dose calibrator after the cell washing step, and the initial dose refers to the initially treated radioactivity of [^{89}Zr]Zr(oxinate)$_4$.

MTS assay was performed to determine the cytotoxicity of radiolabeled THP-1 cells for up to 7 days. Radiolabeled THP-1 cells were prepared in a 96-well plate, as shown in **Table. 1** below, and cytotoxicity was confirmed on the same day. As a control, the same number of non-radiolabeled THP-1 cells were prepared.

Table 1. Initial cell number of radiolabeled THP-1 for daily cytotoxicity assay

Days	Radiolabeled THP-1 cells
0	1×10^5 cells
1	5×10^4 cells
3	5×10^4 cells
5	1×10^4 cells
7	1×10^4 cells

2.2.8. *In vivo* cell trafficking by PET imaging

Animal experiments were conducted with the approval of the Institutional Animal Care and Use Committee (IACUC, approval number BA-2111-332-008-03). BALB/c nude mice (male, six weeks old) were purchased from Orient Bio (South Korea), and after a one-week incubation period, they were reared in a specific pathogen-free (SPF) environment. Water and chow were fed *ad libitum* under a normal night/day cycle of 12 hours.

The tail vein of the mice was injected with 5×10^6 radiolabeled, armed THP-1 cells (~ 740 KBq). PET/CT images were acquired using small animal PET/CT (NanoPET/CT, Mediso Inc., Hungary) at 2 hours, 1, 4, and 6 days after injection. PET images were analyzed using PMOD software (version 3.6, PMOD Technologies Ltd., Switzerland).

2.2.9. Statistical analysis

The results are presented as mean ± standard deviation (SD). Means between the two groups were compared using Student's two-tailed *t*-test, whereas the one-way ANOVA was used for comparison when more than two groups were compared. p values < 0.05 were considered statistically significant. Statistical analyses were performed using the GraphPad Prism 8.0 software (GraphPad Software Inc., CA, USA).

2.3. Results and discussion

2.3.1. *In vitro* cytotoxicity assay

Treatment with Ac_4ManNAz at concentrations ranging from 5 to 100 μM did not significantly increase cytotoxicity compared to the control group. (**Figure 2.1**).

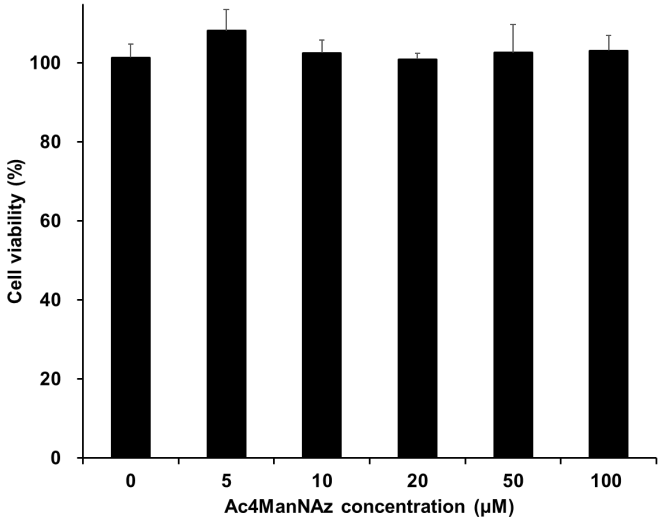

Figure 2.1 *In vitro* cytotoxicity of THP-1 cells at various concentrations of $Ac_4ManNAz$.

Next, an assessment of the effect of the cytotoxicity of DBCO-Cy5.5 on THP-1 cells was conducted. THP-1 cells were treated for 1 h with DBCO-Cy5.5 (0, 5, 10, 20, 50, and 100 μM), and cytotoxicity was evaluated. Treatment with DBCO-5.5 at 5–100 μM concentration resulted in no significant cytotoxicity compared to the control group (**Figure 2.2**).

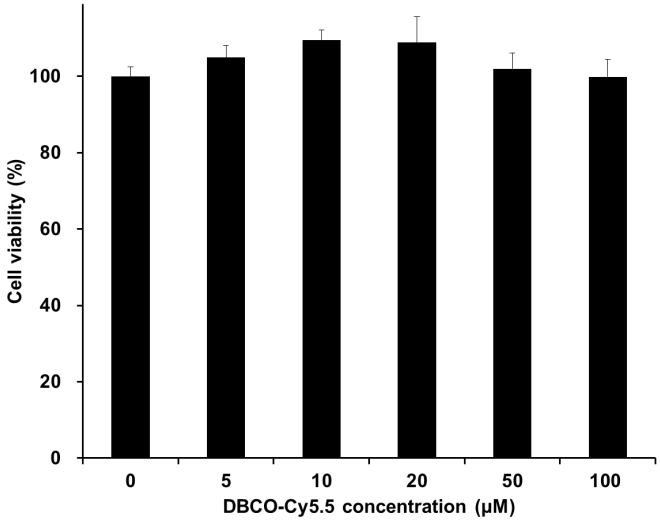

Figure 2.2 *In vitro* cytotoxicity of THP-1 cells at various concentrations of DBCO-Cy5.5.

Metabolic glycoengineering is a novel technology that can enable the expression of reactive chemical groups on the cell surface using cellular metabolism. It has the advantage of easily conjugating new functional groups to reactive groups formed on cell membranes by bioorthogonal chemical reactions. This experiment confirmed that there was no cytotoxicity caused by substances used in metabolic glycoengineering (Ac_4ManNAz or DBCO-bearing fluorophore). Accordingly, the optimal treatment concentration of Ac_4ManNAz was set at 100 μM.

2.3.2. *In vitro* cell-surface azide expression and bioorthogonal labeling of THP-1 cells

THP-1 cells treated with Ac_4ManNAz were conjugated with DBCO-Cy5.5 using bioorthogonal labeling. The cells were treated with 100 μM Ac_4ManNAz to achieve maximal expression of azide without cytotoxicity. The non-toxic concentration of DBCO-Cy5.5 for bioorthogonal labeling was also determined by evaluating treatments with several concentrations of DBCO-Cy5.5 (0, 5, 10, 20, 50, and 100 μM).

Confocal fluorescence microscopy and flow cytometry were conducted to estimate the fluorescence signal intensity of Cy5.5 on the cell surface (**Figure 2.3**), which was determined to increase in a dose-dependent manner. The treatment concentration of ADIBO-GUL (100 μM), which exhibited no cytotoxicity and is advantageous for bioorthogonal labeling, was optimized and applied to the next experiment.

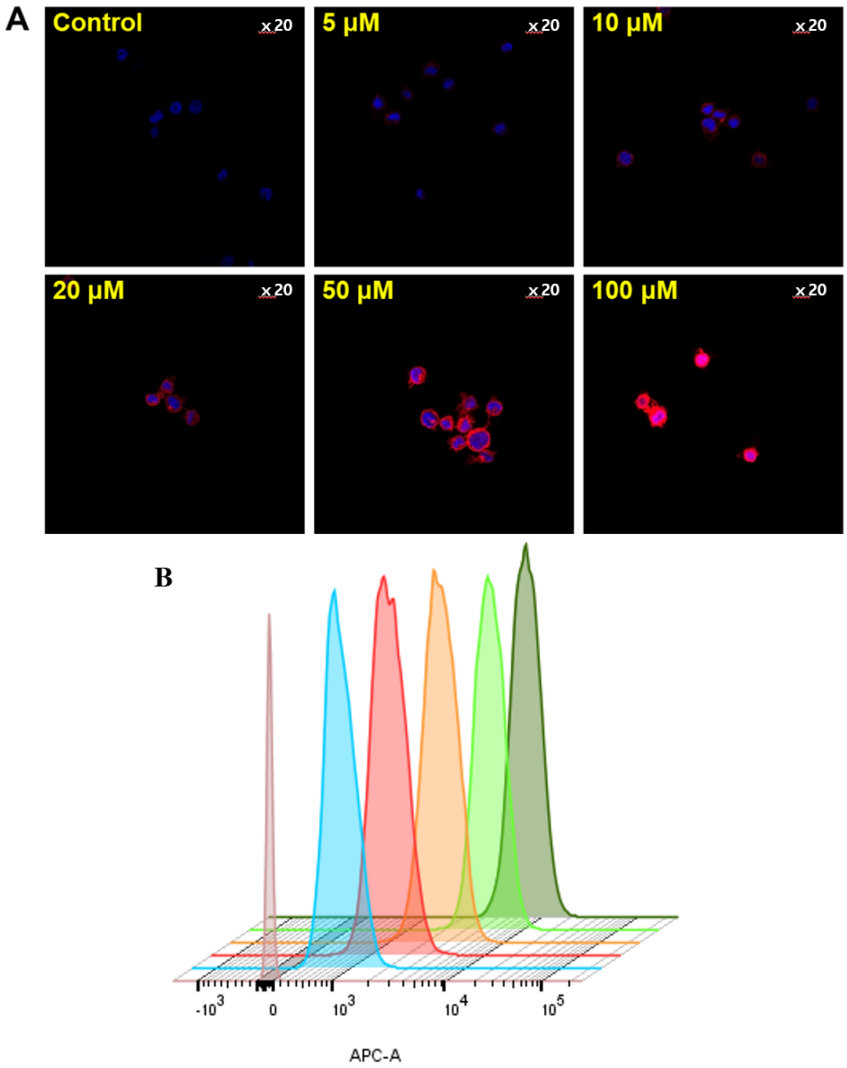

Figure 2.3 Differences in the efficiency of bioorthogonal labeling according to the DBCO-Cy5.5 treatment concentration. (A) Confocal microscopy analysis of Ac_4ManNAz treated THP-1 cells after DBCO-Cy5.5 conjugation at various concentrations. The cell nuclei were stained with DAPI(blue). The merged image showed Cy5.5(red) localized on the cellular membrane. (B) Flow cytometric assay of Ac_4ManNAz treated THP-1 cells after DBCO-Cy5.5 conjugation at various concentrations. Fluorescence intensity increased in a dose-dependent manner of DBCO-Cy5.5 .

In the bioorthogonal chemical reaction, it was confirmed that the fluorescence signal of conjugated Cy5.5 increased up to 100 μM in a dose-dependent manner. Based on these results, the treatment concentration of ADIBO-GUL was also set to 100 μM.

2.3.3. Cell-to-cell gluing test

The cell-to-cell gluing test was performed to evaluate adhesion to target cells (22RV1) using THP-1 cells conjugated with ADIBO-GUL instead of DBCO-Cy5.5. To conjugate the PSMA targeting motif to THP-1 cells, they were treated with 100 μM of Ac_4ManNAz for 24 h, followed by 100 μM ADIBO-GUL for 1 h. Cell-to-cell gluing to 22RV1 cells was confirmed using the PSMA targeting motif armed THP-1 cells as effector cells.

Non-armed THP-1 cells used as a control did not show adhesion to either PC3 or 22RV1 cells. Armed THP-1 cells also did not show adherence to PC3 cells. On the other hand, it was confirmed that a large number of armed THP-1 cells were attached and specifically bound to 22RV1 (**Figure 2.4**). This phenomenon is considered to have influenced the interaction with 22RV1 cells by endowing THP-1 cells with a PSMA targeting ability that did not previously exist.

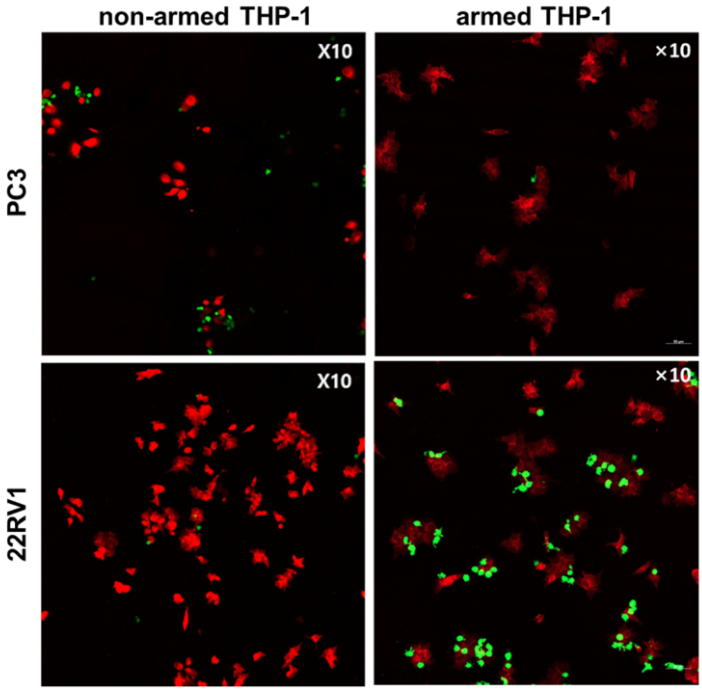

Figure 2.4 Cell-to-cell gluing test. Target cells(PC3 and 22RV1 cells) were stained with Far-Red dye(red), and effector cells(THP-1 cells) were stained CFSE(green), respectively.

2.3.4. [^{89}Zr]Zr(oxinate)$_4$ synthesis cell radiolabeling

The radio-TLC profile of [^{89}Zr]Zr(oxinate)$_4$ synthesis is shown in **Appendix Figure A1**. The [^{89}Zr]Zr(oxinate)$_4$ complex was synthesized in an aqueous solution and was used for cell labeling without further purification.

Cells were radiolabeled using [^{89}Zr]Zr(oxinate)$_4$ to monitor the trafficking of the injected cells *in vivo* using PET imaging. To determine cytotoxicity by cell radiolabeling, 5×10^6 cells of THP-1 cells were labeled with 0.74 MBq or 7.4 MBq of [^{89}Zr]Zr(oxinate)$_4$. Non-radiolabeled THP-1 cells were used as a negative control. In the low-activity labeled group, cell viability significantly increased compared to the control group on days 1 and 3 after radiolabeling, and there was no difference from the control group until seven days. In the high-activity labeled group, cell proliferation was temporarily increased on day 1 after radiolabeling, but it was not significant. However, from day 3 after radiolabeling, the cell viability decreased dramatically, and cytotoxicity was determined by radiolabeling (**Figure 2.5**). According to these results, cell radiolabeling was performed in subsequent experiments under low activity conditions. At low activity labeling conditions, a labeling efficiency of 54.5 ± 17.8% for [^{89}Zr]Zr(oxinate)$_4$ was determined.

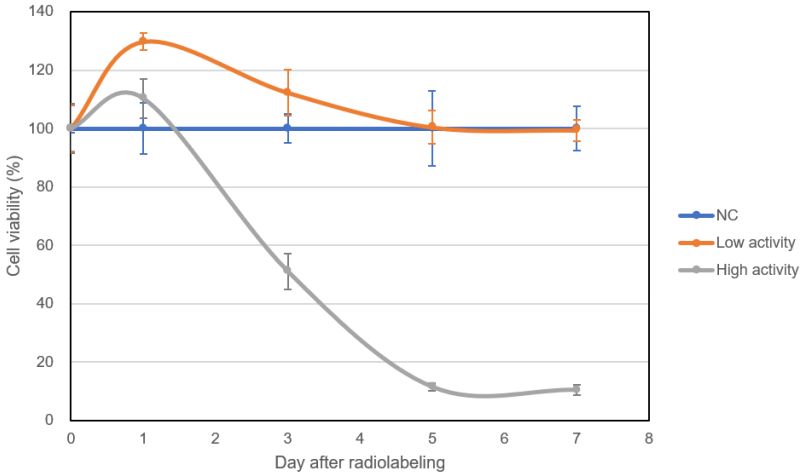

Figure 2.5 Cytotoxicity of radiolabeled cells at different radioactivity conditions. Radiolabeling under low activity conditions significantly increased cell viability until day 3 and, after that, showed no difference from the negative control. However, under high activity conditions, it was determined that cell viability was slightly increased on day 1 and then decreased rapidly by cytotoxicity.

2.3.5. *In vivo* cell trafficking using PET imaging

PET/CT images were obtained at 2, 24, 96, and 144 hours after injection. Radiolabeled, armed THP-1 cells migrated to the lung 2 h after injection and were detected to be distributed throughout the lung until day 6. It was established that some radioactively labeled armed THP-1 cells migrated to the liver and spleen from day 1 after injection, and it was established that the amount of migration to the liver and spleen gradually increased until day 6 (**Figure 2.6**).

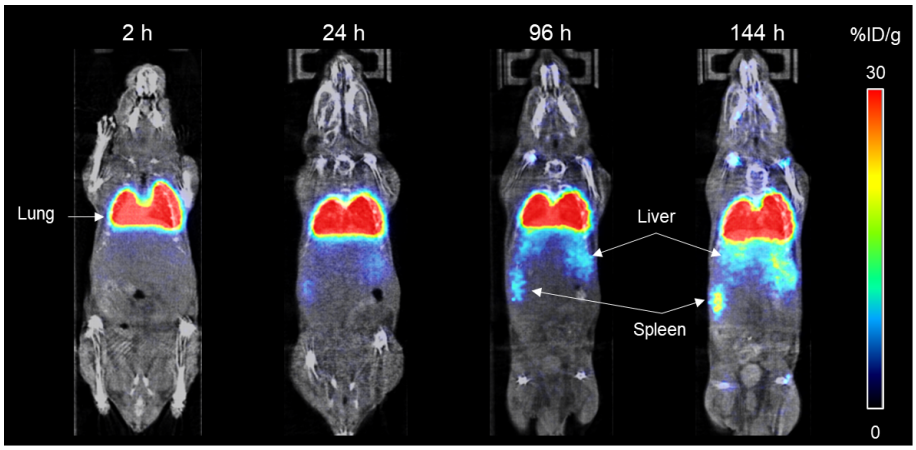

Figure 2.6 Representative small animal PET/CT images at 2, 24, 96, and 144 h after injection of radiolabeled armed THP-1 cells in normal mice.

It was reported that the concentration of eGFP-5T33 cells radiolabeled with [^{89}Zr]Zr(oxinate)$_4$ peaked at 9 h after injection and then declined thereafter [30]. In another report, [^{89}Zr]Zr-DFO-Bn-NCS-labeled leukocytes were confirmed to remain in the lungs up to 4 hours after the injection before migrating to the liver and spleen, which continued until day 7. It was determined that human mesenchymal stem cells radiolabeled in the same manner remained in the lungs for up to 7 days [31]. This study determined that the radiolabeled armed THP-1 cells stayed in the lungs and then gradually moved to the liver and spleen. However, compared to previous reports, significant amounts of the injected cells were identified in the lungs up to 6 days after injection. Considering these results, using an actual prostate cancer tumor transplantation animal model may limit target cell migration. This phenomenon is presumed to be the death of injected cells or their stagnation without passing through pulmonary capillary vessels, and the cells maintained in the lungs need to be identified histologically.

2.4.Summary

In this study, the concentration of Ac_4ManNAZ was optimized using a cytotoxicity test. In addition, using the cytotoxicity test results and flow cytometric assay, it was confirmed that the in vitro bioorthogonal labeling increased in a dose-dependent manner for DBCO-Cy5.5 concentrations up to 100 μM. Next, the PSMA-specific targeting ability of armed THP-1 cells was confirmed by labeling them using ADIBO-GUL instead of DBCO-Cy5.5. This phenomenon is considered to have influenced the interaction with 22RV1 cells by endowing THP-1 cells with a PSMA targeting ability that did not previously exist.

The $[^{89}Zr]Zr(oxinate)_4$ complex was synthesized in an aqueous solution and was used for cell labeling without further purification. Cells were radiolabeled using $[^{89}Zr]Zr(oxinate)_4$ to monitor the trafficking of the injected cells in vivo by PET imaging. 5×10^6 THP-1 cells were labeled with low (~ 0.74 MBq) or high (~ 7.4 MBq) activity $[^{89}Zr]Zr(oxinate)_4$, and non-radiolabeled THP-1 cells as a control. Low activity conditions did not cause any cytotoxicity to the THP-1 cells. However, cell viability in the high-activity labeled group was dramatically decreased by $[^{89}Zr]Zr(oxinate)_4$ until day 7. According to these results, cell radiolabeling was performed in a subsequent experiment under low activity conditions, and at this time, the labeling efficiency for $[^{89}Zr]Zr(oxinate)_4$ was observed to be 54.5 ± 17.8%.

PET/CT images were obtained at 2 hours, 1, 4, and 6 days after injection using small animal PET/CT. Armed THP-1 cells migrated to the lung at 2 h after injection and continued migrating throughout the lung until day 6. After that, it was confirmed that armed THP-1 cells migrated to the liver and spleen from day 1, and the migration gradually increased.

Chapter 3. Conclusion

This study demonstrated that PSMA-targeting ligands that were conjugated to THP-1 cells through metabolic glycoengineering and bioorthogonal chemistry were specifically bound to PSMA-positive cell lines. The small animal PET/CT images helped monitor the in vivo behavior of radiolabeled THP-1 cells. Based on the results of this study, it is expected that metabolic glycoengineering can be used to improve the targeting ability of immunomodulatory cell therapy products, evaluate in vivo pharmacokinetics, and predict drug distribution using cell tracking imaging techniques.

Appendix

Figure A1. Radio-TLC profiles for [^{89}Zr]Zr(oxinate)$_4$ synthesis

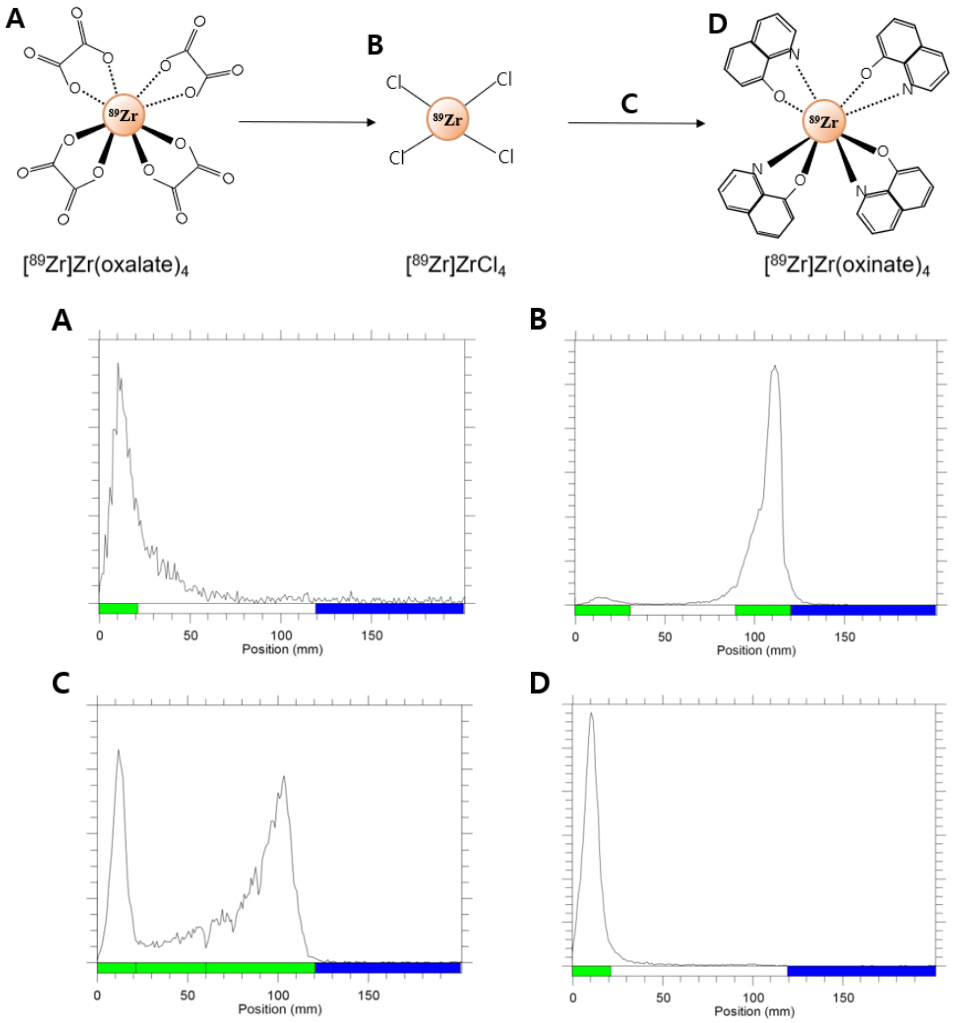

Radio-TLC profiles on silica gel instant thin-layer chromatography paper (ITLC-SG; Agilent Technologies) in 50 mM DTPA. (A) The radio-TLC result of [^{89}Zr]Zr(oxalate)$_4$; (B) [^{89}Zr]ZrCl$_4$; (D) [^{89}Zr]Zr(oxinate)$_4$. (C) Radio-TLC results were obtained during the process of converting [^{89}Zr]ZrCl$_4$ to [^{89}Zr]Zr(oxinate)$_4$.

References

1. Zinzani PL. Traditional treatment approaches in B-cell non-Hodgkin's lymphoma. Leuk Lymphoma. 2003 Nov 1;44(Suppl 4):S6–14.
2. June CH, O'Connor RS, Kawalekar OU, Ghassemi S, Milone MC. CAR T cell immunotherapy for human cancer. Science. 2018 Mar 23;359(6382):1361–5.
3. Porter DL, Levine BL, Kalos M, Bagg A, June CH. Chimeric antigen receptor-modified T cells in chronic lymphoid leukemia. N Engl J Med. 2011 Aug 25;365(8):725–33.
4. Hamieh M, Dobrin A, Cabriolu A, van der Stegen SJC, Giavridis T, Mansilla-Soto J, et al. CAR T cell trogocytosis and cooperative killing regulate tumour antigen escape. Nature. 2019 Apr;568(7750):112–6.
5. Majzner RG, Mackall CL. Tumor antigen escape from CAR T-cell therapy. Cancer Discov. 2018 Oct;8(10):1219–26.
6. Glover M, Avraamides S, Maher J. How can we engineer CAR T cells to overcome resistance? Biologics. 2021 May 19;15:175–98.
7. Strohl WR, Naso M. Bispecific T-cell redirection versus chimeric antigen receptor (CAR)-T cells as approaches to kill cancer cells. Antibodies (Basel). 2019 Jul 3;8(3).
8. Adachi K, Kano Y, Nagai T, Okuyama N, Sakoda Y, Tamada K. IL-7 and CCL19 expression in CAR-T cells improves immune cell infiltration and CAR-T cell survival in the tumor. Nat Biotechnol. 2018 Apr;36(4):346–51.
9. Zhang Z, Lu M, Qin Y, Gao W, Tao L, Su W, et al. Neoantigen: A new breakthrough in tumor immunotherapy. Front Immunol. 2021 Apr 16;12:672356.
10. Takayama Y, Kusamori K, Nishikawa M. Click chemistry as a tool for cell engineering and drug delivery. Molecules. 2019 Jan 4;24(1).

11. Park J, Andrade B, Seo Y, Kim M-J, Zimmerman SC, Kong H. Engineering the surface of therapeutic “living” cells. Chem Rev. 2018 Feb 28;118(4):1664–90.
12. Yoon HI, Yhee JY, Na JH, Lee S, Lee H, Kang SW, et al. Bioorthogonal copper free click chemistry for labeling and tracking of chondrocytes in vivo. Bioconjug Chem. 2016 Apr 20;27(4):927–36.
13. Rahmim A, Zaidi H. PET versus SPECT: strengths, limitations and challenges. Nucl Med Commun. 2008 Mar;29(3):193–207.
14. Rodriguez-Porcel M. In vivo imaging and monitoring of transplanted stem cells: clinical applications. Curr Cardiol Rep. 2010 Jan;12(1):51–8.
15. Fischer G, Seibold U, Schirrmacher R, Wängler B, Wängler C. (89)Zr, a radiometal nuclide with high potential for molecular imaging with PET: chemistry, applications and remaining challenges. Molecules. 2013 Jun 3;18(6):6469–90.
16. Sato N, Wu H, Asiedu KO, Szajek LP, Griffiths GL, Choyke PL. (89)Zr-oxine complex PET cell imaging in monitoring cell-based therapies. Radiology. 2015 May;275(2):490–500.
17. Deri MA, Zeglis BM, Francesconi LC, Lewis JS. PET imaging with ^{89}Zr: from radiochemistry to the clinic. Nucl Med Biol. 2013 Jan;40(1):3–14.
18. Minn I, Huss DJ, Ahn H-H, Chinn TM, Park A, Jones J, et al. Imaging CAR T cell therapy with PSMA-targeted positron emission tomography. Sci Adv. 2019 Jul 3;5(7):eaaw5096.
19. Maresca KP, Hillier SM, Femia FJ, Keith D, Barone C, Joyal JL, et al. A series of halogenated heterodimeric inhibitors of prostate specific membrane antigen (PSMA) as radiolabeled probes for targeting prostate cancer. J Med Chem. 2009 Jan 22;52(2):347–57.
20. Lütje S, Heskamp S, Cornelissen AS, Poeppel TD, van den Broek SAMW, Rosenbaum-Krumme S, et al. PSMA ligands for radionuclide imaging and

therapy of prostate cancer: clinical status. Theranostics. 2015 Oct 18;5(12):1388–401.

21. Debnath S, Zhou N, McLaughlin M, Rice S, Pillai AK, Hao G, et al. PSMA-targeting imaging and theranostic agents-current status and future perspective. Int J Mol Sci. 2022 Jan 21;23(3).

22. Kozikowski AP, Zhang J, Nan F, Petukhov PA, Grajkowska E, Wroblewski JT, et al. Synthesis of urea-based inhibitors as active site probes of glutamate carboxypeptidase II: efficacy as analgesic agents. J Med Chem. 2004 Mar 25;47(7):1729–38.

23. Holmberg AR, Marquez M, Lennartsson L, Meurling L, Nilsson S. Synthesis and binding of a novel PSMA-specific conjugate. Anticancer Res. 2018 Mar;38(3):1531–7.

24. Kwon H, Son S, Byun Y. Prostate-specific membrane antigen (psma)-targeted radionuclide probes for imaging and therapy of prostate cancer. Asian J Org Chem. 2019 Sep;8(9):1588–600.

25. Rørth P. Communication by touch. Cell. 2003 Mar;112(5):595–8.

26. Fry TJ, Shah NN, Orentas RJ, Stetler-Stevenson M, Yuan CM, Ramakrishna S, et al. CD22-targeted CAR T cells induce remission in B-ALL that is naive or resistant to CD19-targeted CAR immunotherapy. Nat Med. 2018 Jan;24(1):20–8.

27. Slaney CY, von Scheidt B, Davenport AJ, Beavis PA, Westwood JA, Mardiana S, et al. Dual-specific chimeric antigen receptor T cells and an indirect vaccine eradicate a variety of large solid tumors in an immunocompetent, self-antigen setting. Clin Cancer Res. 2017 May 15;23(10):2478–90.

28. Koo H, Choi M, Kim E, Hahn SK, Weissleder R, Yun SH. Bioorthogonal click chemistry-based synthetic cell glue. Small. 2015 Dec 22;11(48):6458–66.

29. Laughlin ST, Agard NJ, Baskin JM, Carrico IS, Chang PV, Ganguli AS, et al. Metabolic labeling of glycans with azido sugars for visualization and glycoproteomics. Glycobiology. 2006 Jan 1;415:230–50.

30. Charoenphun P, Meszaros LK, Chuamsaamarkkee K, Sharif-Paghaleh E, Ballinger JR, Ferris TJ, et al. [(89)Zr]oxinate4 for long-term in vivo cell tracking by positron emission tomography. Eur J Nucl Med Mol Imaging. 2015 Feb;42(2):278–87.

31. Bansal A, Sharma S, Klasen B, Rösch F, Pandey MK. Evaluation of different ^{89}Zr-labeled synthons for direct labeling and tracking of white blood cells and stem cells in healthy athymic mice. Sci Rep. 2022 Sep 19;12(1):15646.

국문 초록

세포치료제는 줄기세포 또는 면역세포 등 세포를 기반으로 하는 치료법이다. 특히, 면역조절세포치료제는 수지상세포(dendritic cell), 자연살해 세포(natural killer cell), T 세포 등의 면역세포를 이용하여 면역반응을 활성화시켜 질병 치료에 사용되는 의약품이다. 면역조절세포치료제 중 최근 임상적으로 활발히 연구가 진행되고 있는 CAR-T 는 키메릭 항원 수용체(chimeric antigen receptors, CARs)를 발현하는 유전자를 T 세포에 도입하여 발현하는 개념으로, 현재 국외에서도 승인이 기대되는 신기술 분야이다. 그러나 이러한 CAR-T 치료법 역시 충분한 표적화가 이루어지지 않을 경우 on-target/off-tumor effect 의 부작용으로 인한 한계점도 가지고 있다. 이러한 표적능의 한계와 부작용을 극복하기 위해 이중특이성(bispecific) CAR-T 를 개발하거나 CAR 의 성능과 효능을 향상시키기 위한 노력이 이루어지고 있다.

이러한 CAR-T 세포와 같은 면역세포치료의 문제점을 극복하기 위해서는 면역세포와 종양세포 간의 상호작용(cell-cell interaction)이 중요하며, 특히 이는 세포 표면의 리간드와 수용체 간의 결합이 중요하게 작용한다. 예로, CAR-T 에 이용되고 있는 CD20, CD22, HER2 등이 종양세포의 표적화에 이용되고 있다. 이러한 두 세포들 간의 결합이 강화되면 보다 효과적인 항암치료를 기대할 수 있다. 최근 당대사공학(metabolic glycoengineering)을 사용하여 세포 표면에서 당구조물의 발현을 조절한 다음, 생물직교 화학(bioorthogonal “click” chemistry)를 사용하여 인공적인 표적 리간드와 같은 구조를 결합하는 방법이 제시되고 있다.

당대사공학은 인공 당과 당단백질 합성과정을 이용하여 세포 표면에 화학적 표지가 가능한 수용체를 도입할 수 있는 기술이다. Azide 반응기는 N-azifoacetyl-mannosamine(Ac_4ManNAz) 등의 기질을 이용하여 화학적 표지를 위해 세포 표면에 형성될 수 있다. 이후 생물직교 화학반응으로 결합이 가능한 다양한 구조물을 쉽고 빠르게 시험관 내 또는 생체내에서 결합할 수 있는 장점이 있다.

본 학위 논문의 목표는 당대사공학 및 "클릭 반응"을 이용하여 면역세포치료제에서 전립선특이막항원(prostate specific membrane antigen, PSMA)에 대한 표적화 능력을 높이고 PET 영상을 이용하여 세포추적을 시각화하는 것이다.

THP-1 세포를 다양한 농도(0, 5, 10, 20, 50, 100 μM)의 Ac_4ManNAz 와 함께 24 시간 동안 처리하여 세포 표면에 반응성 작용기를 발현시켰다. 당대사조작된 세포를 DBCO-bearing fluorophore (ADIBO-Cy5.5)를 이용하여 1 시간 동안 다양한 농도조건(0, 5, 10, 20, 50, 100 μM)에서 처리하여 염색하였다. 이를 공초점 형광 현미경 및 유세포 분석법을 이용하여 분석을 진행함으로써 당대사공학 및 클릭 반응을 이용하여 THP-1 세포의 표면에서 생체직교 결합이 일어남을 확인하였다. THP-1 세포의 표면에 PSMA 표적화 리간드를 무장시키기 위해 Ac_4ManNAz 가 처리된 THP-1 세포에 최종농도 100 μM 의 DBCO-PSMA ligand (ADIBO-GUL)를 처리하고 1 시간 배양하였다. 세포 인식에 대한 효과를 평가하기 위해, PSMA 리간드가 무장된 THP-1 세포(작용 세포)와 PSMA 양성 종양세포인 22RV1 세포 또는 PSMA 음성 종양세포인 PC3 세포(표적 세포)를 Effector-to-target 비율 3:1 로 공동배양 하였다. 이때 THP-1 세포(작용 세포)와 표적 세포 사이의 상호작용을 공초점 형광 현미경을 이용하여 확인하였고, PSMA 표적구조를 포함하지 않은 THP-1 세포를

음성 대조군으로 이용하였다. $[^{89}Zr]Zr(oxinate)_4$ 는 음이온 교환 카트리지르 이용하여 oxalate 구조로부터 합성되었다. 합성된 $[^{89}Zr]Zr(oxinate)_4$ 의 친유성을 확인하기 위해 LogD7.4 가 측정되었다. 이후 방사성 표지된 THP-1 세포를 준비하기 위해, ~740 kBq 수준의 $[^{89}Zr]Zr(oxinate)_4$ 를 이용하여 5×10^6 개의 세포를 표지하였다. 방사성 표지된 세포는 감마 카운터를 이용하여 세포에 표지된 방사능을 측정하였고, MTS 방법을 이용하여 최대 7 일까지의 세포 생존능을 확인하였다. $[^{89}Zr]Zr(oxinate)_4$ 로 방사성 표지된 PSMA 표적 리간드 무장 THP-1 세포를 정상 마우스의 꼬리 정맥을 통하여 투여한 뒤 2 시간, 1, 4, 6 일에 각각 PET 영상이 획득되었다.

세포독성시험에서, THP-1 세포는 Ac_4ManNAz 또는 ADIBO-Cy5.5 의 최대 처리 농도인 100 μM 까지 어떠한 독성도 확인되지 않았다. 공초점 형광 현미경 영상과 유세포 분석법에서, THP-1 세포는 ADIBO-Cy5.5 의 처리용량에 비례한 효율적 표지를 확인하였다. 효율적 세포 표면 표지에 대한 최적농도로써 100 μM 이 이후 실험에서 사용되었다. 작용 세포와 표적 세포 사이의 결합은 PSMA 음성인 PC3 세포에서 관찰되지 않았다. 22RV1 세포에서도 음성 대조군으로 사용된 THP-1 세포와의 세포 간 결합이 나타나지 않았다. 하지만 PSMA 리간드 무장 THP-1 세포와 22RV1 세포 사이의 세포 간 결합이 확인되었으며, 이는 두 가지 유형의 세포 사이에서 세포 표면의 표적화 리간드에 의한 세포 간 인식이 일어남을 보여준다. $[^{89}Zr]Zr(oxinate)_4$ 의 LogD7.4 측정값은 1.47 ± 0.02 로, 친유성을 확인하였고, 세포 방사성 표지 효율은 54.4 ± 17.8%였다. 단일 세포 당 0.09 ± 0.03 Bq 로 표지된 THP-1 세포는 방사성 표지 후 7 일까지 방사성 표지가 되지 않은 대조군 THP-1 세포와 비교하여 유의한 세포독성을 나타내지 않아 방사성 표지에 의한 세포 독성은 확인되지

않았다. 마우스에 투여된 THP-1 세포는 가장 먼저 폐에 높은 비율로 축적되었다가, 이후 시간이 지남에 따라 점차 간, 비장 등의 다른 장기로 이동함을 확인하였다.

위 방법을 통하여 PSMA 표적 세포를 준비하기 위해 100 μM 의 $Ac_4ManNAz$ 를 처리하고, PSMA 표적 리간드(ADIBO-GUL)를 이용하여 효율적으로 세포를 무장할 수 있음을 성공적으로 입증하였다. 또한 $[^{89}Zr]Zr(oxinate)_4$ 를 이용하여 세포에 대한 독성 없이 세포를 방사성 표지할 수 있음을 확인하였다. 이는 PSMA 리간드 무장 세포 요법이 세포 표적화 능력을 개선하고 PET 영상을 이용하여 세포의 체내 이동을 추적할 수 있음을 제안하였다.

주요어: 세포치료제, 전립선특이막항원(PSMA), 당대사공학, 클릭화학, 세포추적, PET
학 번: 2019-27624